Polymer 51 (2010) 3293–3302

Contents lists available at ScienceDirect

Polymer

journal homepage: www.elsevier.com/locate/polymer

Effect of chain stiffness on the morphology of polyelectrolyte complexes. A Monte Carlo simulation study

C.F. Narambuena [a,b,*], E.P.M. Leiva [a], M. Chávez-Páez [b], E. Pérez [b]

[a] Departamento de Matemática y Física, Facultad de Ciencias Químicas, Universidad Nacional de Córdoba, Haya de la Torre y Medina Allende, Ciudad Universitaria, 5000 Córdoba, Argentina
[b] Instituto de Física, Universidad Autónoma de San Luis Potosí, Av. Manuel Nava 6, Zona Universitaria, 78290 San Luis Potosí, SLP, México

ARTICLE INFO

Article history:
Received 12 February 2010
Received in revised form
24 April 2010
Accepted 27 April 2010
Available online 7 May 2010

Keywords:
Polyelectrolyte complex
Morphology
Simulation

ABSTRACT

We have employed Monte Carlo simulations and a coarse grain model in order to analyze the final structure and morphology of complexes arising from the interaction between fully-flexible polycations and polyanions with different chain stiffness. Different morphologies, like globules, toroids and rods, are obtained depending on chain stiffness. It was observed that longer chains yield more frequently toroids than rods, as compared with shorter chains. However, the size of toroids does not depend entirely on the chain length. This suggests that the final structure of the toroids is highly dependent on the intrinsic rigidity of chain rather than on the electrostatic contributions.

1. Introduction

Polyelectrolytes (PEs) are polymer chains that, in aqueous dissolution, acquire a certain amount of electrical charge on their monomers. PE solutions show remarkable physicochemical properties as compared with those of the neutral polymer [1], such as the formation of complexes in solution between oppositely charged polyelectrolytes [2] and the adsorption of polyelectrolyte on charged surfaces [3]. Electrostatic interactions and the release of counterions play a key role in the properties of polyelectrolytes [4–6]. In particular, complex formation on surfaces by alternate adsorption with oppositely charged polyelectrolyte causes self-assembling into multilayer films [7]. These structures have been also been developed using biological components to design drug delivery systems [8] and functionalized surfaces [7].

The self-assembling of PE films has been investigated through their surface morphology by atomic force microscopy (AFM) in Liquid-Cell [9], and a granular structure formed by PE complexes has been identified [10]. However, PE complexes forming toroids have also been observed during sequential adsorption of polyethylenimine (PEI) and poly sodium 4-styrenesulfonate (PSS) on glass surfaces [11,12]. Additionally, Stokke et al. have studied the morphology of the semiflexible biological polyanion alginate, acetan, DNA, xanthan, and complexed with chitosan using tapping mode AFM identifying linear, toroidal and globular morphological structures. The results have confirmed that chain stiffness plays a decisive role in the determination of complex structures [13]. These authors have also studied the ability of various chitosans, differing in the fractional content of acetylated units and the degree of polymerizations to compact DNA. Complexes made by mixing plasmid DNA with chitosans yielded a population of toroids and rods [14]. The relative importance of valence and charge density of the polycation chitosan on the compaction process of DNA and xanthan has been also analyzed [15].

A phenomenon closely related to complex formation is DNA condensation by a multivalent salt, in which DNA undergoes a dramatic transition from an extended structure to a compact highly ordered structure [16]

Experiments have shown that morphology of complexes depends on chain stiffness, in which flexible polymers generally collapse to disordered globules, and stiff ones collapse to ordered structures such as toroids or folded chains [17,18].

Hence, it is important to analyze how the physical phenomenon of DNA complex formation by interaction with polycations is related to DNA condensation that takes place by addition of polyvalent ions. Over the last decades, these phenomena have attracted the interest of biophysicists and biochemists. Biologically, the quest to understand DNA toroid formation has been motivated by its

* Corresponding author. Departamento de Matemática y Física, Facultad de Ciencias Químicas, Universidad Nacional de Córdoba, Haya de la Torre y Medina Allende, Ciudad Universitaria, 5000 Córdoba, Argentina. Tel./fax: +54 0351 4344972.
E-mail address: claudionarambuena@fcq.unc.edu.ar (C.F. Narambuena).

0032-3861/$ – see front matter © 2010 Elsevier Ltd. All rights reserved.
doi:10.1016/j.polymer.2010.04.065

relevance to gene packing in certain viruses, and by the potential use of DNA toroids in artificial gene delivery (e.g., gene therapy). DNA condensation has also attracted the attention of polymer physicists, as the collapse of DNA molecules into well-defined structures represents a good example of polymer phase transition.

In numerical simulations of semiflexible polyelectrolyte condensation by addition of polyvalent ions [19–21], the formation of globule, toroidal and rod structures has been observed. But also, reported computational simulation studies where the complexation is carried out between oppositely charged chains, we differentiate between fully flexible [4,22–24] and semiflexible polyelectrolyte chains [25–27]. Guskova et al. have investigated the structure and stability of complexes formed by oppositely charged rigid-chain macromolecules, and their response to variation of external conditions using molecular dynamics [27]. They have found that the chains involved in a complex may have diverse conformations such as toroids, tennis rackets, etc.

In the present work, we will extend these results and study in detail the chain stiffness of our model neutral and charged polymers as a function of their parameters. Then, we will study the effect of chain stiffness and size on the structure the polyelectrolyte complexes, assessing in particular the probability of finding a given morphological structure. We will analyze in detail the local structure of the complexes obtained.

This article is organized as follows: Sections 2 and 3 describe the computational model and the measured quantities respectively. Section 4.1 characterizes the conformation and stiffness of polyelectrolyte chains depending on the different conditions of the model. The polyelectrolyte complex is studied in Section 4.2. Section 5 provides conclusions and remarks.

2. Computational model

We use a primitive model for monomers and small ions. The solvent is modeled in terms of a dielectric continuum, i.e., an implicit solvent with relative dielectric constant $\varepsilon_r = 78$. The simulation box is a cubic one with the dimensions $L \times L \times L$. Periodic boundary conditions are applied in the three directions. The neutral, anionic and cationic polymers are made of N_{pol}, N_{pa} and N_{pc} chains, each with Nm_{pol}, Nm_{pa} and Nm_{pc} monomers, respectively.

The monomers are modeled as charged spheres with a diameter $d = 4$ nm. Two consecutive monomers in each chain are connected by a harmonic stretching spring whose potential energy is assumed to be $u_{\mathrm{bond}} = k_{\mathrm{eq}}(l - l_0)^2$, where l is the bond length and $l_0 = 0.5$ nm is the equilibrium bond length. The spring constant has a value $k_{\mathrm{eq}} = 1000(k_{\mathrm{b}}T/nm^2)$ where k_{b} is Boltzmann's constant, and T is the absolute temperature. This constant is chosen to be high enough so as prevent fluctuations of the bond length.

The intrinsic stiffness of the neutral polymer is modeled by a bending potential energy of harmonic type $u_{\mathrm{bend}} = k_{\mathrm{bend,\ poly}}(\beta - \beta_0)^2$, where β is the angle defined by three consecutive monomers and β_0 is the equilibrium angle value equal to π. The value of the bending constant $k_{\mathrm{bend,\ poly}}$ is varied from 0 to 50 with units in $k_{\mathrm{b}}T/\mathrm{rad}^2$. The equivalent for the polyanion and polycation chain is $u_{\mathrm{bend}} = k_{\mathrm{bend,\ pa}}(\beta - \beta_0)^2$ and $u_{\mathrm{bend}} = k_{\mathrm{bend,\ pc}}(\beta - \beta_0)^2$ respectively.

All the small ions of the system are considered to be rigid spheres with a diameter of $d = 0.4$ nm with an embedded unit (positive or negative) charge. A PE chain has $Nm_{\mathrm{pc}} \times f$ counterions, where f is the fraction of charged monomers in the PE ($f = 1$ in this work), yielding a total number of $N_{\mathrm{cpc}} = N_{\mathrm{pc}} \times Nm_{\mathrm{pc}} \times f$ counterions when all the PE chains are the polycations and $N_{\mathrm{cpa}} = N_{\mathrm{pa}} \times Nm_{\mathrm{pa}} \times f$ counterions when all the PE chains are the polyanions.

The pair interactions are assumed to be electrostatic and of the hard-sphere type according to:

$$\begin{aligned} u(\vec{r}_{ij}) &= \frac{Z_i Z_j e^2}{4\pi\varepsilon_0\varepsilon_r r_{ij}}, \quad r_{ij} > d \\ u(\vec{r}_{ij}) &= \infty, \quad r_{ij} \le d \end{aligned} \tag{1}$$

where Z_i is the charge of the particle (monomer ion), e is the elemental charge, $\varepsilon_0\varepsilon_r$ is the permittivity of the dielectric continuum, $\vec{r}_{ij}$ is the relative position vector, $r_{ij} = |\vec{r}_{ij}|$ is the distance between particles i and j. The electrostatic energy of the box is calculated with the Ewald summation method [28,29].

The equilibrium properties of the system were evaluated by computer simulations devised according to the Metropolis Monte Carlo (MC) algorithm [30]. The particles were initially positioned at random within the simulation box, avoiding overlapping, since these are represented as hard spheres, according to equation (1). The algorithm employed allowed for single particle displacement, as usual in liquid-state simulations [28,29]. In addition, system equilibration is achieved by taking into account the translational motion of the PE chain with its condensed ionic atmosphere, PE pivot motion, and flip motion of the chains [31]. These moves are accepted with the probability $\{1, \exp(-\Delta U/k_{\mathrm{b}}T)\}$ where ΔU denotes the change of the potential energy between the initial and the final configurations.

The number of free ions of the system was adjusted automatically by means of a Grand Canonical MC (GCMC) procedure [32]. In this work we assume salt free conditions. When the simulation is performed with a single type of polyelectrolyte chain, its counterions are the only small ions present in the system; otherwise in the simulation of a polyelectrolyte complex the GCMC algorithm eliminates all neutral pairs of small ions.

The system was allowed to equilibrate for 10^6 MC steps for a polyelectrolyte chain and 10^7 MC steps for a polyelectrolyte complex, following the evaluation run during 10^6 and 10^7 MC steps respectively.

3. Measured quantities

The rigidity of the polyelectrolyte chain is an important variable influencing the final morphology of polyelectrolyte complexes, thus, it is worth characterizing the conformation of a single chain and complexes morphologies as a function of the parameters that determine the chain stiffness (bending constant and electric charge).

The degree of flexibility was quantified using two kinds of parameters. The first one focuses on the overall flexibility of the chain: quantities derived from the end-to-end vector. The other one, emphasizes on the local flexibility; they are the intrinsic and electrostatic persistent lengths obtained from the segment orientational correlation function, as defined below.

The end-to-end vector $\vec{R}_e = \vec{r}_N - \vec{r}_1$ joining the two ends of the chain was used to characterize the global configuration of the chain. We calculated the mean square of the end-to-end vector $\langle \vec{R}_e^2 \rangle$, obtained by averaging over all conformations. The end-to-end vector $\vec{R}_e$ can be rewritten as:

$$\vec{R}_e = \sum_{i=1}^{Nm-1} \vec{a}_i, \tag{2}$$

where $\vec{a}_i = \vec{r}_{i+1} - \vec{r}_i$ is the segment or bond between the positions of neighboring monomers. Its mean square can be written as follows:

$$\left\langle \vec{R}_e^2 \right\rangle = \left\langle \sum_{i=1}^{Nm-1} \vec{a}_i \cdot \sum_{j=1}^{Nm-1} \vec{a}_j \right\rangle = \sum_{i=1}^{Nm-1} \langle \vec{a}_i \rangle + 2 \sum_{1<i<j<Nm-1} \sum \langle \vec{a}_i \vec{a}_j \rangle \tag{3}$$

The angle θ_{ij} between the vectors a_i and a_j is obtained from the equality:

$$\vec{a}_i \cdot \vec{a}_j = |\vec{a}_i| \cdot |\vec{a}_j| \cos\theta_{ij} \tag{4}$$

When the polymer behaves as an ideal chain (negligible bending potential and zero monomer volume), the segment directions are not correlated and the angle θ_{ij} takes, with equal probability, any value from 0 to π so that the averaging becomes:

$$\langle \vec{a}_i \cdot \vec{a}_j \rangle = l_0^2 \langle \cos\theta_{ij} \rangle = 0 \tag{5}$$

where $l_0 = \langle |\vec{a}_i| \rangle$. Thus, in the case of an ideal chain, equation (3) yields:

$$\left\langle \vec{R}_e^2 \right\rangle = (Nm-1) l_0^2 \tag{6}$$

For a long polymer ($Nm_{poly} \gg 1$) the mean size of an ideal chain is given by the root-mean-square end-to-end distance R_e: [33]

$$R_e = \langle \vec{R}_e \rangle^{1/2} \sim l_0\, Nm^{1/2} \tag{7}$$

In the general case R_e is written as:

$$R_e \sim Nm^{\nu} \tag{8}$$

where ν is a scaling coefficient with a value of 1/2 for an ideal chain and 0.6 for a neutral chain with exclusion volume interactions [34].

Another parameter that will be analyzed is the end-to-end distance D_{ee} defined as $D_{ee} = \sqrt{\vec{R}_e^2}$. After allowed system equilibration, the D_{ee} was calculated from the chain conformations obtained in the Monte Carlo simulations; the end-to-end distance probability distribution density $P(D_{ee})$ was estimated from a histogram.

The segment orientational correlation between two links $\vec{a}_i$ and $\vec{a}_j$ was also calculated according to:

$$\langle \cos\theta_{ij} \rangle = \left\langle \frac{\vec{a}_i \cdot \vec{a}_j}{|\vec{a}_i| \cdot |\vec{a}_j|} \right\rangle \tag{9}$$

If we average over all pairs i, j maintaining constant the value of $s = |i-j|$.

$$\langle \cos\theta(s) \rangle = \left\langle \frac{\vec{a}_i \cdot \vec{a}_j}{|\vec{a}_i| \cdot |\vec{a}_j|} \right\rangle_{s=|i-j|} \tag{10}$$

where $\langle \cos\theta(s) \rangle$ represents the average of the cosine of the angle between the chain segments separated by the length s, called segment orientational correlation function (SOCF).

The morphology of the structures obtained in the polyelectrolyte complex simulations was characterized by the asphericity A. This parameter is useful to measure the anisotropy and deviation from sphericity and is defined as [35]

$$A = \frac{(\lambda_1-\lambda_2)^2 + (\lambda_2-\lambda_3)^2 + (\lambda_1-\lambda_3)^2}{2(\lambda_1+\lambda_2+\lambda_3)^2} \tag{11}$$

where λ_1, λ_2 and λ_3 are the three eigenvalues of the gyration tensor of the chain calculated by

$$\tau_{\alpha,\beta} = \frac{1}{Nm} \sum_{i=1}^{Nm} (\vec{r}_i - \vec{r}_{cm})_\alpha (\vec{r}_i - \vec{r}_{cm})_\beta \tag{12}$$

where the subscripts α and β denote the three Cartesian components x, y and z

The values of A range between 0 and 1. It is equal to 0 for a perfect sphere, 0.25 for a perfect ring, and 1 for a straight line. For an ideal chain, $\langle A \rangle$ is 0.431, as obtained from simulations [36].

The three eigenvalues λ_1, λ_2 and λ_3 of the gyration tensor are the three principal radii of gyration squared Rg_1^2, Rg_2^2 and Rg_3^2 respectively [35]. An invariant of matrix $\tau_{\alpha,\beta}$ is the trace related to the radius of gyration RG [35] by:

$$RG^2 = tr\left(\tau_{\alpha,\beta}\right) = \lambda_1 + \lambda_2 + \lambda_3 = Rg_1^2 + Rg_2^2 + Rg_3^2 \tag{13}$$

The largest eigenvalue is defined as λ_{max} which corresponds to radii gyration maximum squared value Rg_{max}^2:

$$Rg_{max}^2 = \lambda_{max} \tag{14}$$

The radius of a toroid R_{Toroid} has been defined as the root-mean-square of the largest of the three principal radii of gyration.

$$R_{Toroid} = \left\langle Rg_{max}^2 \right\rangle^{1/2} \tag{15}$$

4. Results and discussion

4.1. Conformational and persistence length of a single polyelectrolyte chain

Polymer chains may be characterized by a degree of flexibility and may be categorized into three main groups: flexible chains, in which bending is limited over the length of a few links; semiflexible chains, in which bending becomes appreciable over larger lengths; and rigid rods, where the extension of the bending radius is considerably greater than the chain dimension [33]. In our computational model the chain stiffness is determined by the bending constant and the forces caused by the presence of electrostatic charges on the monomers of the polyelectrolyte.

In Fig. 1, we compare these two contributions to the chain stiffness. The figure shows the dependence of the root-mean-square end-to-end distance R_e on the number of monomers in the chain Nm for a neutral polymer and for a polyelectrolyte with different values of the bending constant. It also shows the maximum chain stretching indicated by the *contour length* of the polymer chain $L_{chain} = (Nm_{pol} - 1) \times l_0$ for qualitative comparison. In order to verify the accuracy of the MC algorithm, we will consider the case of the ideal chain. Within statistical error, the root-mean-square end-to-end distance is found to follow the scaling relations (equation (8)) with $\nu = 1/2$. The results for a neutral polymer with a value of $k_{bend,\ poly} = 0$, the fully flexible case, are found to follow the well-established scaling relations (equation (8)) with $\nu = 0.6$, in good agreement with the theoretical values for an athermal excluded-volume chain [34]. For $k_{bend,\ poly} = 1$–5 the neutral chain has a scaling coefficient $\nu = 0.6$; for higher bending constant values the scaling coefficient increases until it reaches a value of 0.9 approximately. In the polyelectrolyte case, independently of the bending constant the scaling coefficient has a value $\nu \approx 1$, showing that the root-mean-square end-to-end distance is approximately linear with the monomer number in the chain. However, in the case of the polyelectrolyte chain with $k_{bend,\ pa} = 0$, the value of the root-mean-square end-to-end distance is much lower than that of the *contour length*, implying that the polyelectrolyte chain is not fully stretched.

To establish the relationship between the global conformation of the chain and local stiffness we analyzed the end-to-end distance probability distribution density $P(D_{ee})$ for a neutral chain of 60 monomers ($Nm_{pol} = 60$) and a polyanion chain of 60 monomers ($Nm_{pa} = 60$), depicted in Fig. 2a and b, respectively, at different bending constants.

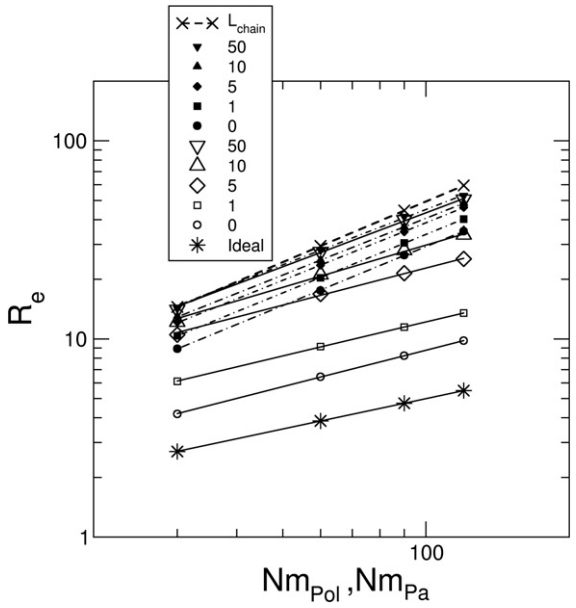

Fig. 1. Plot of the modulus of the end-to-end vector R_e as a function of the number of monomers in the chain for a neutral polymer (empty symbols) and for a polyelectrolyte (filled symbols). The different values of bending constant k_{bend} are given inside the figure.

Fig. 2a shows the effect of the bending constant $k_{bend,\ poly}$ on $P(D_{ee})$ for a neutral polymer, where the most probable values of D_{ee} can be compared with the *contour length* for this chain size $L_{chain} = 29.5$ nm. For a value of $k_{bend,\ poly} = 0$, the fully flexible case, the values of D_{ee} present a symmetric distribution with a maximum value of $P(D_{ee})$ close to 6 nm. This is much smaller than the contour length of the chain, implying that in the simulated polymer structures, stretched conformations constitute a minor fraction, while the major fraction corresponds to forms strongly coiled in space. We also note that the fluctuations in the values of D_{ee} have the same order of magnitude as its average value, implying that under the present conditions D_{ee} is a strongly fluctuating property. Increasing the chain stiffness $k_{bend,\ poly} = 1$–10 give us the semiflexible case, where the function $P(D_{ee})$ shifts to higher D_{ee} values. Fig. 2a shows meaningful fluctuations around the maximum value. These fluctuations are drastically reduced when $k_{bend,\ poly} = 50$, where the most probable conformation corresponds to a fully extended structure, with a maximum value close to the contour length.

Wilhelm and Frey [37] have calculated analytically the end-to-end distance distribution function of a semiflexible polymer adopting a continuum wormlike chain model. They obtained the following expression:

$$G(d_{ee}) = \frac{2\,\kappa}{4\,\pi\,N}\sum_{n=1}^{\infty}\pi^2 n^2(-1)^{n+1}e^{-\kappa\pi^2 n^2(1-d_{ee})} \qquad (16)$$

where $d_{ee} = D_{ee}/L_{chain}$ is the end-to-end distance relative to the chain contour length, N is a normalization constant, $\kappa = l_p^0/L_{chain}$, where l_p^0 is the intrinsic persistence length. Fig. 2a shows in full line the $G(d_{ee})$ obtained by fitting equation (16) in comparison with $P(D_{ee})$ obtained from our Monte Carlo simulations. The curves fitting process considered only one free parameter, l_p^0. The general observation is that equation (16) reproduces the data qualitatively well and is an excellent approximation for $k_{bend,\ poly} \geq 1$. The values of l_p^0 at a given $k_{bend,\ poly}$ are weakly dependent on the chain size, therefore, we averaged the value of l_p^0 on the different chain sizes. Table 1 displays the average values of l_p^0, where a linear relationship between l_p^0 and $k_{bend,\ poly}$ can be observed.

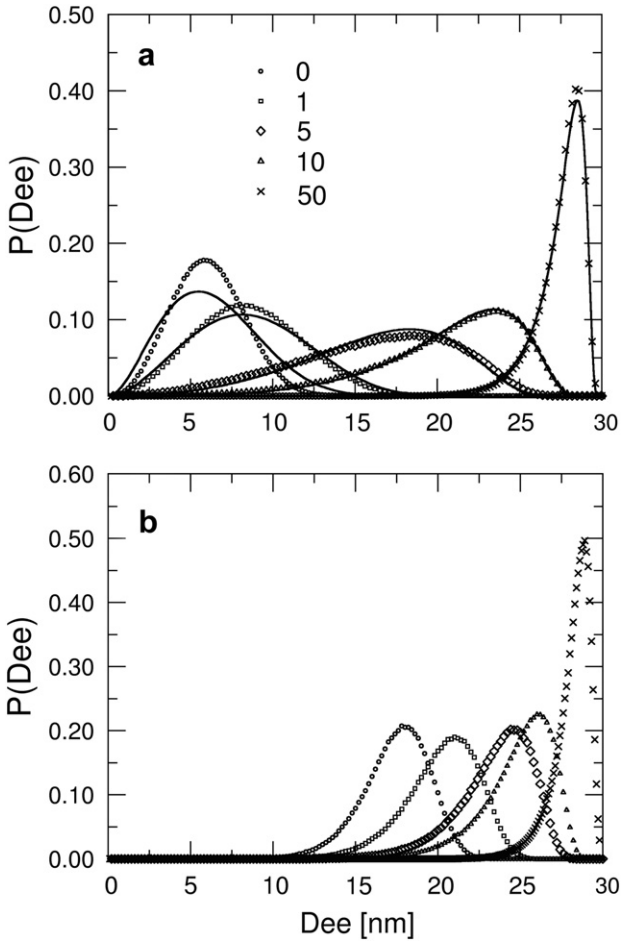

Fig. 2. End-to-end distribution function $P(D_{ee})$ for a chain of 60 monomers at different bending constants as obtained from Monte Carlo simulation (symbols) and using $G(d_{ee})$ of Equation (16) (solid line). (a) Neutral chain (b) Polyanion chain. The values of bending constants are given in the upper figure.

Fig. 2b shows the combined effects of bending potential and electrostatic interaction on $P(D_{ee})$ for a polyanion chain of 60 monomers. In the case of $k_{bend,\ pa} = 0$ the change of $P(D_{ee})$ is relatively abrupt as compared with the neutral case present in Fig. 2a. $P(D_{ee})$ is shifted to greater D_{ee} values, but the most probable values of D_{ee} are still far from the chain contour length. This suggests that, although electrostatic interactions tend to stretch the polymer

Table 1
Intrinsic (l_p^0) and electrostatic (l_p^e) persistence length values for neutral polymer and polyanion chains at different bending constant and sizes. The values are given in nm and correspond to fits using equations (16), (17) and (20) as indicated in the corresponding columns.

	l_p^0		l_p^e			
k_{bend}	(eq. (16))	(eq. (17))	($Nm_{pa} = 30$) (eq. (20))	($Nm_{pa} = 60$) (eq. (20))	($Nm_{pa} = 90$) (eq. (20))	($Nm_{pa} = 120$) (eq. (20))
0	0.8	0.4	10.3	25.3	43.1	59.6
1	1.3	1.4	10.5	26.2	45.1	61.5
2	2.0	2.5	10.8	26.6	46.2	64.1
4	3.8	4.8	10.8	26.9	46.4	64.0
5	4.8	6.0	10.8	27.1	44.5	65.4
10	10.0	11.5	10.6	25.6	44.7	65.0
20	20.2	23.5	9.8	24.5	41.2	58.7
30	32.4	34.8	10.5	23.2	39.7	55.4
40	43.0	46.5	10.5	21.6	39.0	56.3
50	55.6	58.0	10.4	21.2	37.9	52.0

chain, they are not strong enough to yield a rigid rod, in agreement with Fig. 1. When $k_{\text{bend, pa}} = 1$, the $P(D_{ee})$ function shows a similar picture, but at a greater value of the bending constant, $k_{\text{bend, pa}} = 5$ or $k_{\text{bend, pa}} = 10$, the fluctuations are reduced considerably with respect to the neutral polymer case. When $k_{\text{bend, pa}} = 50$, the $P(D_{ee})$ profiles are similar for the neutral and the charged polymer, indicating that under these conditions the intrinsic stiffness dominates. The $P(D_{ee})$ profiles for the polyanion, Fig. 2b, are poorly fitted by equation (16) (data not shown), which means that the polyelectrolyte conformational statistics cannot be satisfactorily interpreted in terms of a wormlike chain model.

We used the SOCF, defined in equation (10), combined with theoretical interpretations to estimate the intrinsic and electrostatic contributions to the persistence length.

Fig. 3 shows the SOCF for a neutral chain (a) and for a polyanion chain (b) of 60 monomers for different values of the bending constant. In the neutral polymer case, the SOCF shows the shape of a simple exponential decay. This can be interpreted in the theoretical framework by the following expression [33]:

$$\langle \cos\theta(s)\rangle = \exp\left(-\frac{s}{l_p^0}\right) \tag{17}$$

where the preexponential factor is equal to unity, because $\cos\theta\,(s=0) = 1$. The curves obtained from the theoretical expression equation (17) can fit satisfactorily the SOCF for $k_{\text{bend, pol}} \geq 1$. Volume

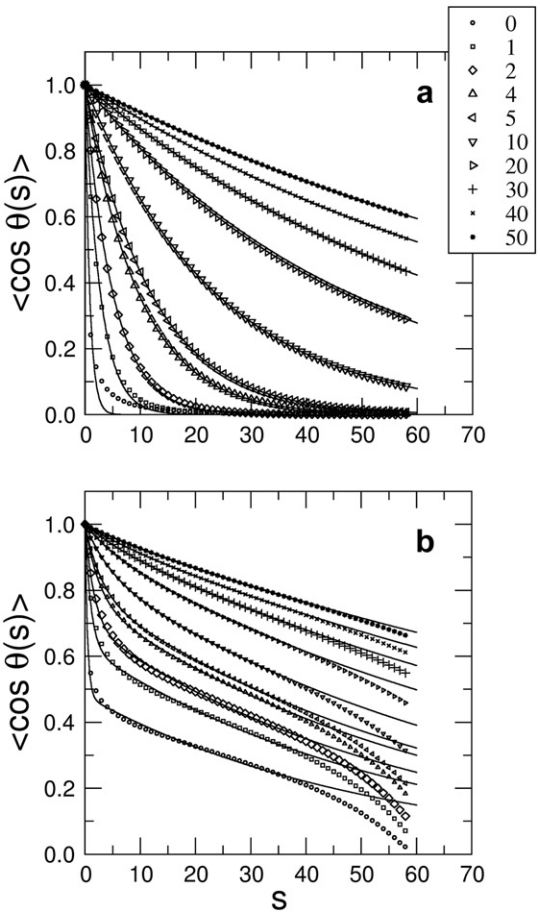

Fig. 3. SOCF of a neutral polymer (a) and a polyanion (b) of 60 monomers. The different values of bending constant used are reported inside the upper graphic. The continuous lines represent the fit with the theoretical expressions (17) and (20) for (a) and (b) respectively.

exclusion effects become important in the limiting case of the fully flexible chain; this effect was not taken into account in the theoretical derivation of equation (17) [33]. The simple exponential decay observed suggests that there is only one relevant spatial scale to characterize the intrinsic persistence length; this is the main feature of the worm-chain model [33]. The l_p^0 values obtained from this fitting were averaged on the different chain sizes and are reported in Table 1. These values are in excellent agreement with those calculated with equation (16).

The SOCF for a polyanion chain, Fig. 3b, is qualitatively different from the simple exponential decay found for the neutral polymer case. The long-ranged nature of the electrostatic interactions and the large number freedom degrees introduced by the counterions originate severe difficulties to the SOCF analytical treatment. Pioneering studies on the influence of electrostatic interactions on polyelectrolyte stiffness were undertaken by Odijk [38] and, Skolnick and Fixman [39] performing a perturbative calculation on a slightly bent rigid charged rod using the Debye–Huckel approximation. They found a simple exponential decay for the SOCF of the type:

$$\langle \cos\theta(s)\rangle = \exp\left(-\frac{s}{l_P}\right) \tag{18}$$

where the total persistence length l_P is:

$$l_P = l_p^0 + l_p^e \tag{19}$$

l_p^0 is the intrinsic persistence length defined above and l_p^e the electrostatic contribution. The concept of a unique persistence length of a polyelectrolyte, applied to a flexible or semiflexible chain has been questioned using computer simulations [40,41]. In the present work, we have obtained no satisfactory fittings to equation (18) for flexible and semiflexible polyelectrolytes. Petra Bacova [42] found a suitable fit for the simulated polyelectrolyte SOCF with a double exponential function:

$$\langle \cos\theta(s)\rangle = B\exp\left(-\frac{s}{l_p^0+l_p^e}\right) + (1-B)\exp\left(-s\frac{l_p^e+(1-B)l_p^0}{l_p^0\left(l_p^0+l_p^e\right)(1-B)}\right) \tag{20}$$

This expression was obtained by Mangui and Netz [43] who considered, in their theoretical study a charged polyelectrolyte, with a Gaussian statistics in a solution of a monovalent salt. The chain was assumed to be of infinite length and the electrostatic interactions were treated at a linear level with a Debye–Hückel screened interaction between charges due to the presence of monovalent counterions and salts. This treatment neglects nonlinear effects connected to counterion condensation [44], as well as chain-end effects [45], present in our simulations. The fitted curves of the simulation results according to equation (20) are shown in Fig. 3b, using the values for l_p^0 obtained with the neutral polymer case. We considered chain segment separations $s \leq 30$, since below this separation the two decays predicted by equation (20) are evident. Above this separation there is a third decay resulting from the effects of chain ends, which were not considered in the derivation of equation (20).

The electrostatic persistence length l_p^e obtained through equation (20) does not vary significantly with the bending constant, but is highly sensitive to the chain size. The approximate l_p^e values are 10, 20, 40, and 60 nm for chains with 30, 60, 90 and 120 monomers respectively. This means that l_p^e has a magnitude comparable to the chain contour length $(Nm_{\text{pol}} - 1) \times l_0$ because in the salt-free conditions the electrostatic interactions have the same reach as the size chain used.

Table 2
Detail of polyelectrolyte complex systems used in the present work.

System	N_{pa}	Nm_{pa}	N_{pc}	Nm_{pc}
*S*1	1	60	2	30
*S*2	1	90	3	30
*S*3	1	120	4	30

4.2. Morphology of polyelectrolyte complex

In order to study the polyelectrolyte complex morphology we have chosen a representative subset of parameters for a first approximation to the problem, with particular emphasis on size and stiffness. We will work with three systems, denoted *S*1, *S*2 and *S*3, as described in Table 2.

Each system is made of a "long" polyanion chain and several "short" polycation chains. The long polyanion chain was given three different sizes: $Nm_{pa} = 60$, 90, 120 for the *S*1, *S*2 and *S*3 systems respectively; it also had variable stiffness governed by the $k_{bend,\ pa}$ values. In the case of the polycation chains, we have considered them as totally flexible chains ($k_{bend,\ pc} = 0$), with $Nm_{pc} = 30$. We added as many short polycation chains as necessary to obtain a system with equal amounts of polycation and polyanion monomers.

Fig. 4 shows several configurations obtained from simulations with different stiffness values of the long chain (red one) combined with the short flexible chains (blue ones). Each panel corresponds to a single trajectory. Panel 4a shows three characteristic structures formed by a fully flexible long chain complexed with shorter chains. The final complex structures present a globular shape. When the long chain stiffness is increased $k_{bend,\ pa} = 4$, the structures are no longer globular and become more stretched, yielding pseudo-toroidal shapes (panel b). With a larger bending constant, $k_{bend,\ pa} = 10$ the presence of toroidal structures becomes evident (panel 4c). Some highly elongated shapes are also found. When we reach extreme rigidity setting $k_{bend,\ pa} = 50$, elongated structures with the shape of rigid rods are formed, but different from those obtained with $k_{bend,\ pa} = 10$. While the latter are obtained by roughly folding the chain in half, yielding an U shaped structure, in the former case the chain is fully extended.

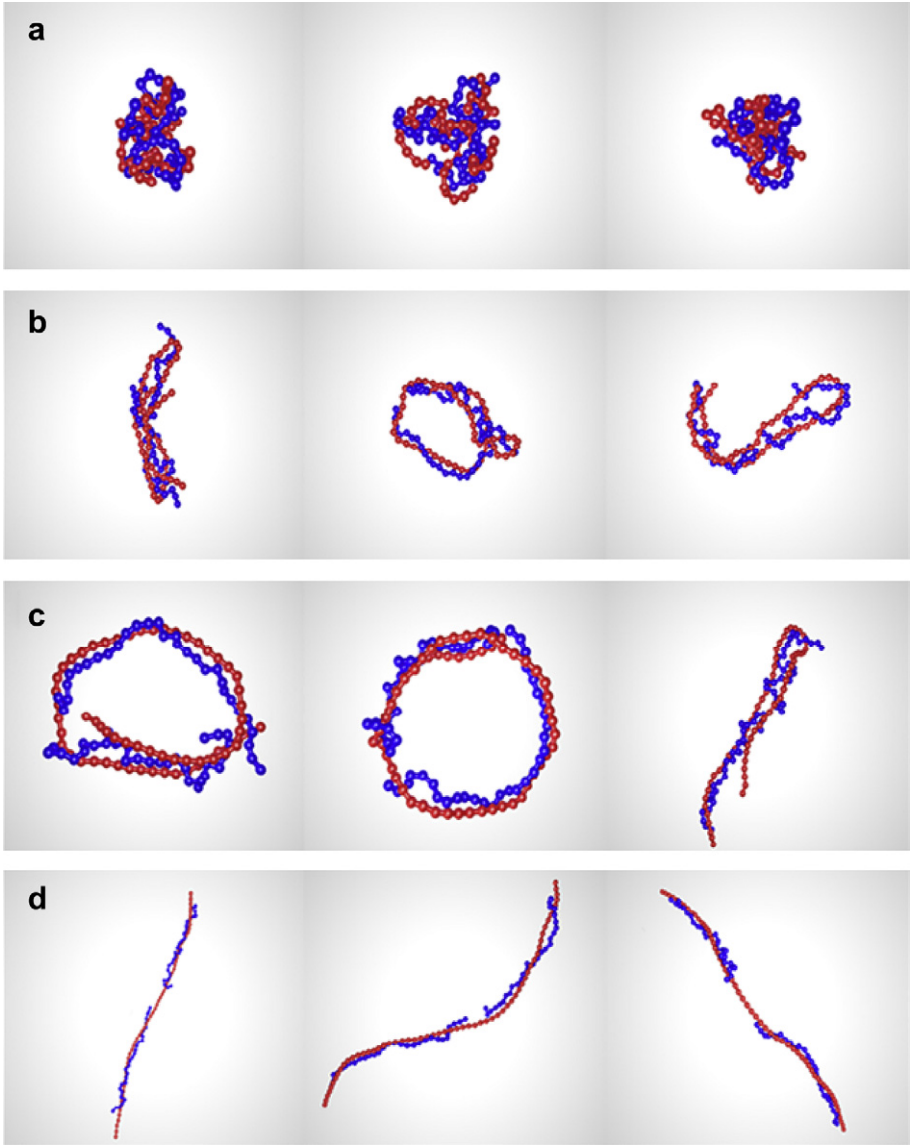

Fig. 4. Typical configurations obtained from the simulations of system *S*1 with different values of the bending constant for the polyanion chain, (a) $k_{bend,\ pa} = 0$, (b) $k_{bend,\ pa} = 4$, (c) $k_{bend,\ pa} = 10$, (d) $k_{bend,\ pa} = 50$. The long polyanion chain contains 60 monomers and the two short fully flexible polycation chains contain 30 monomers each.

A probability density function $P(A)$ can be estimated by building a histogram of asphericity A values from the complex structures obtained from Monte Carlo simulations. We have considered four Monte Carlo separate runs for each histogram, keeping all model and system parameters fixed but changing the random seed and therefore the initial configuration.

Fig. 5 shows three histograms of the asphericity probability density function for complexes of system $S1$ formed by a long chain of 60 monomers, with different bending constants and two short fully flexible chains of 30 monomers each. The values of bending constant were $k_{\text{bend, pa}} = 0$, 10, 50 for Fig. 5a, b, and c respectively.

When the long chain is totally flexible $k_{\text{bend, pa}} = 1$, most asphericity values are below 0.35, Fig. 5a, with maximum values close to 0.1–0.15. These results suggest that under these conditions the complex structures have a globular morphology, of the type shown in Fig. 4a. By increasing polyelectrolyte stiffness values to higher ones, $k_{\text{bend, pa}} = 10$, Fig. 5b, the probability function changes qualitatively. Under these conditions two peaks are obtained in the probability histograms, one around $A = 0.25$ and another close to $A = 0.9$. This means that the complex structures are toroidal or rod-like. If the stiffness of the chain is increased to very high $k_{\text{bend, pa}} = 50$ values, the resulting structures have asphericity values close to unity, evidencing the presence of rod-like structures.

We can summarize the previous information by constructing a diagram which graphically depicts the morphological probabilities as a function of the stiffness of the long chain. The probability of observing a globular structure P_G is defined as:

$$P_G = \sum_{A=0}^{A<0.2} P(A) \tag{21}$$

i.e., as the probability sum of finding structures with A values between 0 and 0.2. Similarly, the probabilities of observing toroids P_T and rods P_R morphologies are defined as:

$$P_T = \sum_{A=0.2}^{A=0.3} P(A) \tag{22}$$

$$P_R = \sum_{A=0.8}^{A=1} P(A) \tag{23}$$

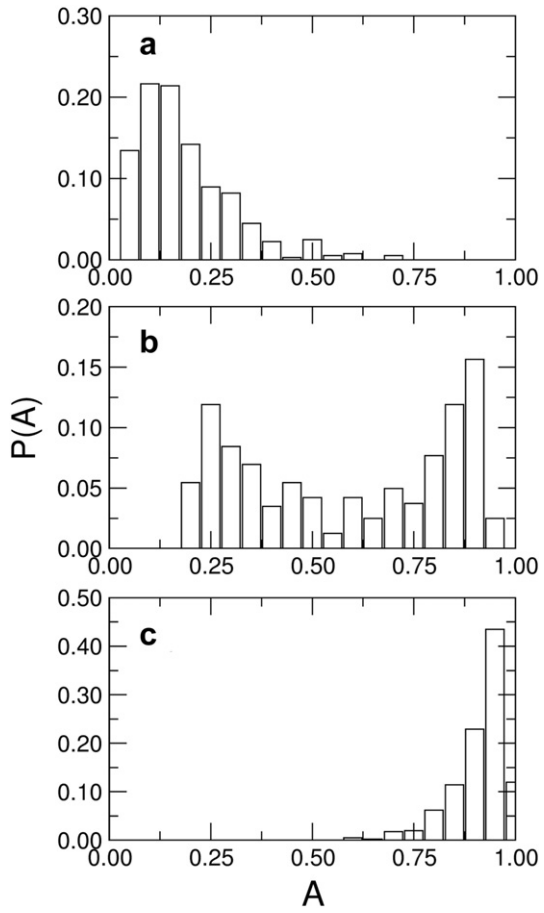

Fig. 5. Histograms of the asphericity probability density for complexes of system $S1$ formed from a long polyanion chain (60 monomers) with different bending constants and two short (30 monomers) fully flexible polycation chains. (a) $k_{\text{bend, pa}} = 0$, (b) $k_{\text{bend, pa}} = 10$, (c) $k_{\text{bend, pa}} = 50$.

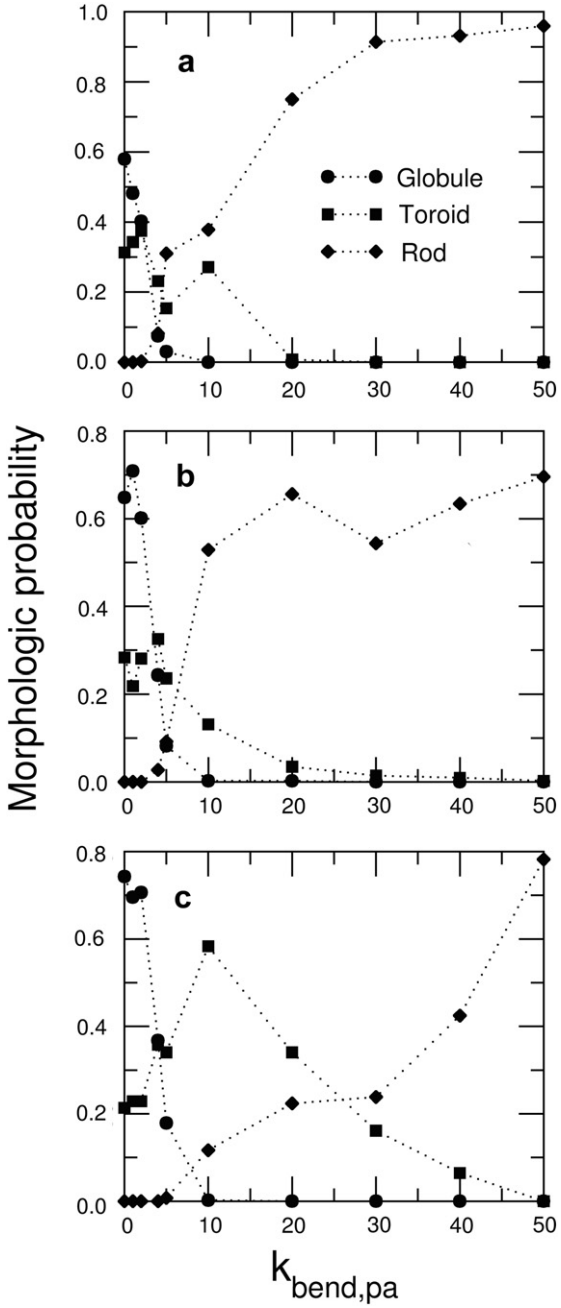

Fig. 6. Probability of obtaining a given type of morphology (globule, toroid, and, rod) as a function of the bending constant for different systems $S1$, $S2$ and, $S3$. Top: $S1$, Middle: $S2$, bottom: $S3$.

Fig. 6 presents the morphologic probabilities P_g, P_T and, P_g of finding a given structure type as a function of the stiffness of the long chain for the different systems. For the *S*1system, Fig. 6a, the long chain with low bending constant $k_{\text{bend, pa}} < 4$, the globular structure is the predominant form observed, but when the long chain is semiflexible $5 < k_{\text{bend, pa}} < 10$, the morphology is more likely to be that of toroids or rods, mainly that of the last. For stiffness corresponding to $k_{\text{bend, pa}} > 10$ only rod structures are observed, in agreement with the qualitative conclusions drawn from the structures of Fig. 4. Fig. 6b shows the plots for the *S*2 system where it can be noticed that its behavior is similar to the system *S*1, with the presence of the morphologies in a comparable relative proportion as a function of the polyanion stiffness. System *S*3 displays certain peculiarities with respect to *S*1 and *S*2. It is remarkable that a mixture of rods and toroids is obtain at $k_{\text{bend, pa}} = 10$, but the predominance of rods is reverted and the toroid morphology is the more likely. This behavior extends up to $k_{\text{bend, pa}} = 20$. In addition, the presence of toroids remains until $k_{\text{bend, pa}} = 40$, denoting that the toroidal stability range increases in the *S*3 system.

In the following discussion we analyze the local structure of the polyanion chain for different complex morphologies obtained for the *S*1 system. This is addressed by calculating the SOCF of the long polyanion chain in the complex for different values of the bending constant $k_{\text{bend, pa}}$, as shown in Fig. 7.

When the long chain is totally flexible, the orientational correlation function decreases to values less than zero and shows a minimum close to $s = 8$ which then increases tending to zero; this correspond to the globular structure. When the stiffness of the chain is increased by setting $k_{\text{bend, pa}} = 4$, a maximum occurs after the minimum, resulting in a functional shape which resembles a damped cosine. The minimum and maximum are approximately localized at $s = 14$ and $s = 33$ respectively. For a higher bending constant ($k_{\text{bend, pa}} = 10$), two types of structures appear, toroids and rods, which have oscillatory and monotonically decreasing behavior respectively, Fig. 7c. The oscillations under this condition are more intense, and the minimum and maximum are close to $s = 19$ and $s = 38$ respectively. Finally, for a very high bending constant, the orientational correlation function becomes very similar to that of a neutral polymer with a similar stiffness. After trying various functional dependencies, it comes out that the previous correlations can be adjusted satisfactorily with a single mathematical expression:

$$\langle \cos\theta(s) \rangle = \cos\left(\frac{s^{\omega}}{A_0}\right) \exp\left(-\frac{s^{\omega}}{A_1}\right) \tag{24}$$

where A_0, A_1 and ω are parameters. The interpretation of this expression and its parameters is beyond the scope of this paper and therefore subject of upcoming work.

As we have seen, polyelectrolyte complexes take a limited number of morphologies, i.e., there are certain morphologies that become more stable depending on the size and rigidity of the chains. In particular, there are conditions where two or more types of morphologies are possible. For example when $Nm_{\text{pa}} = 60$ and $k_{\text{bend, pa}} = 10$ toroids and rods coexist, something which also happens at $Nm_{\text{pa}} = 90$. However, at $Nm_{\text{pa}} = 120$ the range of bending constant values where toroid structures are stable is between $k_{\text{bend, pa}} = 10$–40. This means that these structures have a greater range of stability as the size of the polyanion chain increases. We have analyzed in detail the structure of toroids obtained under different sizes and rigidities of the polyanion chain. In the following discussion, we make a first attempt to correlate the toroid structure formed with the intrinsic persistence length and the electrostatic interactions occurring in the polyanion chains.

Fig. 8a, b and c show three typical complex configurations obtained with polyanion chains with lengths $Nm_{\text{pa}} = 60, 90$ and 120 respectively, upon the addition of polycation chains $Nm_{\text{pc}} = 30$ to neutralize the polyanions (systems *S*1, *S*2, and *S*3, summarized in Table 2). The polyanion has a bending constant of 10. The SOCF for the three complexes shown in Fig. 8 a, b and c is plotted in Fig. 8d. We note that this function has the shape of a damped cosine, with maxima and minima at similar locations. This indicates that the polyanion chain is closed so that it maintains a very similar shape although the size of the polyanion chain is different. A measure of the radius of the toroids can be obtained by averaging the largest eigenvalue of the inertia matrix equation (15). According to this, the calculated radius of the three complexes as a function of the

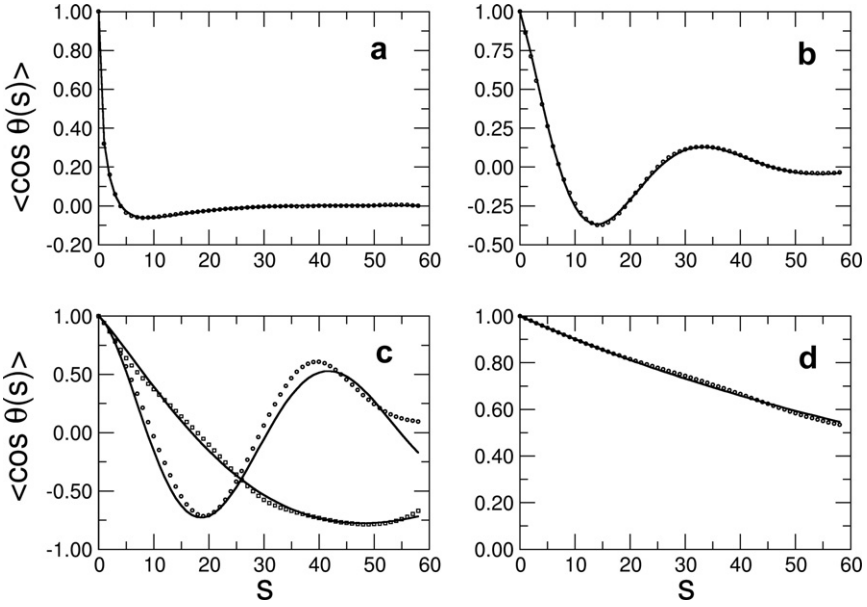

Fig. 7. SOFC for the long polyanion chain in the complex formed in the *S*1 system for different values of its bending constant, (a) $k_{\text{bend, pa}} = 0$, (b) $k_{\text{bend, pa}} = 4$, (c) $k_{\text{bend, pa}} = 10$, (d) $k_{\text{bend, pa}} = 50$.

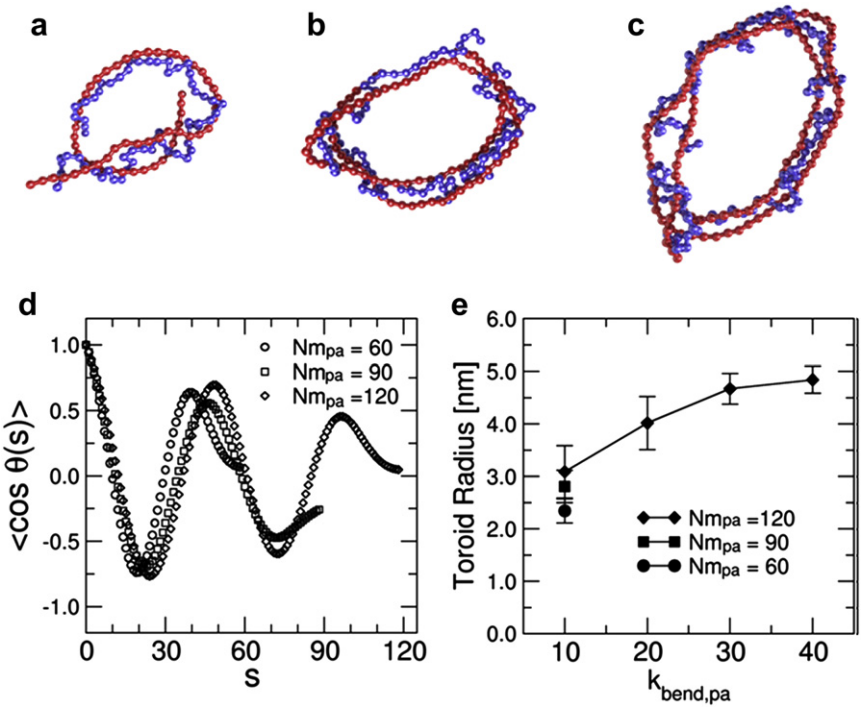

Fig. 8. a), (b) and (c) are typical configurations of toroid systems *S*1, *S*2 and *S*3 respectively. (d) SOFC for the long polyanion chain in the complex formed at the systems*S*1, *S*2 and *S*3 with $k_{\text{bend, pa}} = 10$. (e) Toroid radius for systems *S*1, *S*2 and *S*3 at different bending constants.

bending constant is shown in Fig. 8e. For $k_{\text{bend, pa}} = 10$ we see that the three complexes have radii of the same order 2.3 ± 0.2 nm, 2.8 ± 0.3 nm, 3.0 ± 0.5 nm for *S*1, *S*2 and *S*3 systems respectively. These results suggest that the final structure of the nanotoroids is mainly determined by the intrinsic rigidity of the polyanion chain and not by its size. On the other hand, the electrostatic persistence length, very different for the three systems considered (see Table 1) seems not to play a relevant role. The reason for this may be that this quantity has only a meaning for the isolated polyanion chain, losing its significance when it becomes complexed.

5. Conclusions

We have employed Monte Carlo simulations and a model based on a coarse grain description of polyelectrolytes in order to analyze the existence of complex structures formed from the interaction between polycations and polyanions. In particular, we have studied the effect of chain stiffness on the final structure of resulting complexes. Chain stiffness was controlled by means of an angular harmonic bending potential whose intensity was varied to achieve flexible chains, semiflexible chains and rigid rods. Chain stiffness was characterized by local and global parameters. In this respect, in the case of a neutral polymer, the SOCF was found to exhibit a simple exponential decay, while in the case of the polyelectrolyte it has a more complex behavior that can be approximated by a double exponential, as long as end effects are left aside. After the stiffness characterization, the properties of complex structures were studied by allowing the interaction between a polyanion made of 60, 90 or 120 monomers and totally flexible cationic chains of 30 monomers. This interaction resulted in the formation of different morphologies, like globules, toroids and rods. Generally speaking, when the polyanionic chain is totally flexible, a globular structure appears. When the chain is semiflexible, mixtures of toroids and rods arise, whereas in the rigid case only rods are the most likely formations. The SOCF of the polyanionic chain presents interesting shapes when it is forming part of the complex. It exhibits forms that range from a single minimum for the totally flexible polyanion to a damped cosine for the semiflexible polyanion, or a linear decay for the rigid polyanion. All these correlations may be synthesized into a product made of cosines and an exponential function.

One of the most important factors affecting complex morphology is the chain length of the polyanion. It was observed that longer chains display higher occurrence percentage of toroids than of rods. However the structure of the toroids as characterized by SOCF and the radius do not depend significantly on chain length. This suggests that the final structure of the toroid is more dependent on the intrinsic rigidity of the chain than on the electrostatic contribution. Using rigid chains for the representation of polycation and polianion, Guskova et al. [27] obtained toroids at low temperature and with large chain sizes. We obtained toroids at room temperature, and the probability of observing toroid P_T increased with the chain size. This means that the formation of toroid structures is favored by the mixture of fully flexible and semiflexible chains.

The presence of toroids, rods and globular structures indicates that polyelectrolyte complexes have complicated energy landscapes. Our numerical studies showed that the energies associated with toroid and rodlike structures are comparable in certain circumstances. The next task to be tackled for the present system is the calculation of the free energy for the formation of complex structures, in order to analyze the relative stability of the different morphologies, especially in those ranges of the bending constant where they appear to coexist. This will allow to decide which structure is the real ground state of the polyelectrolyte complexes in the experimental conditions considered.

Another issue to be considered is the dynamics of complex formation. As a more distant goal, we can mention the study of complex formation on charged surfaces, in comparison with the analogous process in solution.

Acknowledgment

C.F. Narambuena wants to thank the financial support of PROMEP Mexico, for postdoctoral grant. We thank Peter Kosovan for information on the SOCF. The computational and technical support by C. Diaz Torrejon and M. Cedillo Torres of CNS-IPICYT and R. Ramirez Carmona, J.C. Sanchez Leanos, J. Renteria Arriaga and J. Limon Castillo of IF-UASLP, as well as language assistance by Carolina Mosconi are gratefully acknowledged. E. Pérez thank to PROMEP for financial support. E.P.M. Leiva wish to thank for financial support to Consejo Nacional de Investigaciones Científicas y Técnicas (CONICET), Secyt UNC, and Program BID 2006 PICT No 946.

References

[1] Radeva T, editor. Physical chemistry of polyelectrolytes. New York: Marcel Dekker; 2001.
[2] Kabanov AV, Bronich TK, Kabanov VA, Yu K, Eisenberg A. Macromolecules 1996;29:6797–802.
[3] Decher G. Science 1997;277:1232–7.
[4] Ou Z, Muthukumar MJ. Chem Phys 2006;124:154902-1–154902-11.
[5] Narambuena CF, Beltramo DM, Leiva EPM. Macromolecules 2007;40:7336–42.
[6] Narambuena CF, Beltramo DM, Leiva EPM. Macromolecules 2008;41:8267–74.
[7] Decher G, Schlenoff JB, editors. Multilayer thin films: sequential assembly of nanocomposite materials. Weinheim, Germany: Wiley-VCH; 2003.
[8] Lvov Y, Antipov AA, Mamedov A, Mohwald H, Sukhorukov GB. Nano Lett 2001;1:125–8.
[9] Menchaca JL, Jachimska B, Cuisinier F, Perez E. Colloids Surf A 2003;222:185–94.
[10] Tristan F, Menchaca JL, Cuisinier F, Perez EJ. Phys Chem B 2008;112:6322–30.
[11] Menchaca JL, Flores H, Cuisinier F, Perez EJ. Phys Condens Matter 2004;16:S2109.
[12] Flores H, Menchaca JL, Tristan F, Gergely C, Perez E, Cuisinier FJG. Macromolecules 2005;38:521–6.
[13] Maurstad G, Danielsen S, Stokke BT. J Phys Chem B 2003;107:8172–80.
[14] Danielsen S, Vårum KM, Stokke BT. Biomacromolecules 2004;5:928–36.
[15] Maurstad G, Danielsen S, Stokke BT. Biomacromolecules 2007;8:1124–30.
[16] Bloomfield VA. Curr Opin Struct Biol 1996;6:334–41.
[17] Arscott PG, Li AZ, Bloomfield VA. Biopolymers 1990;30:619–30.
[18] Plum GE, Arscott PG, Bloomfield VA. Biopolymers 1990;30:631–43.
[19] Stevens MJ. Biophys J 2001;80:130–9.
[20] Ou Z, Muthukumar MJ. Chem Phys 2005;123:074905-1–074905-9.
[21] Wei YF, Hsiao PY. J Chem Phys 2007;127:064901-1–064901-14.
[22] Srivastava D, Muthukumar M. Macromolecules 1994;27:1461–5.
[23] Hayashi Y, Ullner M, Linse P. J Phys Chem B 2004;108:15266–77.
[24] Winkler RG. New J Phys 2004;6:11.
[25] Ziebarth J, Wang Y. Biophysical J 2009;97:1971–83.
[26] Jorge AF, Sarraguça JMG, Dias RS, Pais AACC. Phys Chem Chem Phys 2009;11:10890–8.
[27] Guskova OA, Pavlov AS, Khalatur PG. Polym Sci Ser A 2006;48:763–70.
[28] Allen MP, Tieldesley DJ. Computer simulation of liquids. Oxford, U.K.: Oxford Science Publications; 1992.
[29] Frenkel D, Smit B. Understanding molecular simulation. San Diego, CA: Academic Press; 1996.
[30] Metropolis N, Rosenbluth AW, Rosenbluth MN, Teller AH, Teller E. J Chem Phys 1953;21:1087–92.
[31] Binder K. Monte Carlo and molecular dynamics simulations in polymer science. New York: Oxford University Press; 1995.
[32] Torrie GM, Valleau JP. J Chem Phys 1980;73:5807–16.
[33] Grosberg AY, Khokhlov AR. Statistical physics of macromolecules. New York: American Institute of Physics; 1994.
[34] de Gennes PG. Scaling concepts in polymer physics. Ithaca, NY: Cornell University Press; 1979.
[35] Rudnik J, Gaspari G. J Phys A Math Gen 1986;19:L191–3.
[36] Bishop M, Saltiel CJ. J Chem Phys 1988;88:6594.
[37] Wilhelm J, Frey E. Phys Rev Lett 1996;77:2581–4.
[38] Odijk T. J Polym Sci 1977;15:477–83.
[39] Skolnick J, Fixman M. Macromolecules 1977;10:944–8.
[40] Seidel C, Schlacken H, Müller I. Macromolecular Theory and Simulations 1994;3:333–46.
[41] Micka U, Kremer K. Europhys. Lett. 1997;38:279–84.
[42] Bacova P. Study of persistence length of linear polyelectrolytes in solutions. Bachelor thesis. Czech Republic: Charles University in Prague Faculty of Science; 2008.
[43] Mangui M, Netz RR. Eur Phys J 2004;14:67–77.
[44] Manning GS. Q Rev Biophys 1978;11:179–246.
[45] Limbach HJ, Holm C. J Chem Phys 2001;114:9674–82.